Journal of Chemical Neuroanatomy 69 (2015) 7–12

Contents lists available at ScienceDirect

Journal of Chemical Neuroanatomy

journal homepage: www.elsevier.com/locate/jchemneu

Imaging the time-integrated cerebral metabolic activity with subcellular resolution through nanometer-scale detection of biosynthetic products deriving from ^{13}C-glucose☆

Yuhei Takado [a,b,1,**], Graham Knott [c], Bruno M. Humbel [d], Mojgan Masoodi [e,f], Stéphane Escrig [a], Anders Meibom [a,g,**], Arnaud Comment [b,*]

[a] Laboratory for Biological Geochemistry, School of Architecture, Civil and Environmental Engineering (ENAC), Ecole Polytechnique Fédérale de Lausanne (EPFL), CH-1015 Lausanne, Switzerland
[b] Institute of Physics of Biological Systems, Ecole Polytechnique Fédérale de Lausanne, CH-1015 Lausanne, Switzerland
[c] Centre Interdisciplinaire de Microscopie Electronique, Ecole Polytechnique Fédérale de Lausanne, CH-1015 Lausanne, Switzerland
[d] Electron Microscopy Facility, Université de Lausanne, CH-1015 Lausanne, Switzerland
[e] Nestlé Institute of Health Science, Ecole Polytechnique Fédérale de Lausanne, CH-1015 Lausanne, Switzerland
[f] Department of Nutritional Sciences, Faculty of Medicine, University of Toronto, Toronto, Canada
[g] Center for Advanced Surface Analysis, Institute of Earth Sciences, Université de Lausanne, CH-1015 Lausanne, Switzerland

ARTICLE INFO

Article history:
Received 14 August 2015
Received in revised form 21 September 2015
Accepted 21 September 2015
Available online 25 September 2015

Keywords:
Astrocytes
Glucose
Microscopy
Molecular imaging
Neuronal–glial interaction

ABSTRACT

Glucose is the primary source of energy for the brain but also an important source of building blocks for proteins, lipids, and nucleic acids. Little is known about the use of glucose for biosynthesis in tissues at the cellular level. We demonstrate that local cerebral metabolic activity can be mapped in mouse brain tissue by quantitatively imaging the biosynthetic products deriving from [U-^{13}C]glucose metabolism using a combination of *in situ* electron microscopy and secondary ion mass-spectroscopy (NanoSIMS). Images of the ^{13}C-label incorporated into cerebral ultrastructure with *ca.* 100 nm resolution allowed us to determine the timescale on which the metabolic products of glucose are incorporated into different cells, their sub-compartments and organelles. These were mapped in astrocytes and neurons in the different layers of the motor cortex. We see evidence for high metabolic activity in neurons *via* the nucleus ^{13}C enrichment. We observe that in all the major cell compartments, such as *e.g.* nucleus and Golgi apparatus, neurons incorporate substantially higher concentrations of ^{13}C-label than astrocytes.

1. Introduction

Glucose is the main source of energy for the brain, and the source of building blocks for proteins, lipids, and nucleic acids (Schousboe, 2012). The cerebral anabolic pathways from glucose have been investigated in brain sections and bulk samples using labeling methods with stable or radioactive isotopes (Austin et al., 1972; Ben-Yoseph et al., 1995; Brekke et al., 2012; Vrba, 1964). Measurements using glucose labeled with the radioactive ^{14}C isotope have provided information on the kinetics of incorporation of the glucose-derived carbon into macromolecules such as nucleotides, proteins and lipids (Vrba, 1962). However, little is known about local metabolism and biosynthesis from glucose at the cellular level. To spatially monitor glucose uptake and metabolism *in vivo*, several imaging techniques have been used (Devor et al., 2012; Jin et al., 2014; Walker-Samuel et al., 2013; Wehrl et al., 2013). In particular, efforts to map the ^{14}C cerebral distribution following the injection of [^{14}C]glucose have made use of autoradiographic techniques (Dienel et al., 2002; Sokoloff et al., 1977), but the spatial resolution is relatively poor (>10 μm) and clearly insufficient to localize the ^{14}C signal at the cellular level in the brain (Schmidt and Smith, 2005). It has therefore not been possible to quantitatively measure metabolic activity at the level of individual cells in intact tissue.

☆ This work was supported by the Swiss National Science Foundation (grant number PP00P2_133562 to A.C., and grant number 316030_128692 to BMH for the acquisition of the Helios 650), the Centre d'Imagerie BioMédicale (CIBM) of the UNIL, UNIGE, HUG, CHUV, EPFL, and the Leenards and Jeantet Foundations, and by the Synapsis Foundation. The NanoSIMS instrument was funded in part by an ERC Advanced Grant (grant number 246749 to A.M.) and by the Ecole Polytechnique Fédérale de Lausanne.

* Corresponding author at: Institute of Physics of Biological Systems, Ecole Polytechnique Fédérale de Lausanne, EPFL SB IPSB GR-CO, Station 6, CH-1015 Lausanne, Switzerland.
** Corresponding authors.
E-mail addresses: takado@nirs.go.jp (Y. Takado), anders.meibom@epfl.ch (A. Meibom), arnaud.comment@epfl.ch (A. Comment).
[1] Present address: Biophysics Program, Molecular Imaging Center, National Institute of Radiological Sciences, Chiba, Japan.

http://dx.doi.org/10.1016/j.jchemneu.2015.09.003
0891-0618/

NanoSIMS is a high-resolution ion microprobe that can quantitatively map the spatial distribution of stable isotopes in sections of biological tissue. The typical lateral resolution of NanoSIMS images is around 100 nm (Hoppe et al., 2013; Lechene et al., 2006). By correlating electron microscopy (EM) images, with quantified NanoSIMS maps recorded on the same resin section, isotopic distributions in identified cells, and cellular compartments, can be measured. A recent study performed in rodents has demonstrated that the spatio-temporal dynamics of ^{13}C incorporation into liver and brain glycogen following i.p. administration of uniformly ^{13}C-labeled glucose ([U-^{13}C]glucose) can be monitored using these combined techniques (Takado et al., 2015). The aim of the present study was to measure cerebral glucose metabolism with sub-cellular resolution through the ^{13}C incorporation into mammalian brain ultrastructure from [U-^{13}C]glucose. We investigated the time scale in which glucose is integrated into astrocytes and neurons, and their cellular compartments, in adult mouse primary motor cortex. Our results are discussed in the light of the limitations of the current NanoSIMS technology that does not allow to image cryosamples and therefore restrict the measurements to epoxy-embedded slices, in which macromolecular structures, such as proteins, lipids, and nucleic acids are conserved while soluble metabolites are lost.

2. Materials and methods

2.1. Animal preparation and injection protocol

All experiments were conducted in accordance with guidelines and regulations, in particular the EU Directive 2010/63/EU guidelines, and approved by the local regulatory body of the Canton Vaud, Switzerland (Service de la consommation et des affaires vétérinaires, Affaires vétérinaires, Canton de Vaud, Suisse). The data presented in this study are based on experiments with 14 adult (10–14 week-old) wild-type male NMRI mice maintained on a 12 h dark-light cycle and fed with standard chow. For short timescale experiments ($\leq$3 h), mice were fasted overnight with access to water. A 1.1 M aqueous [U-^{13}C]glucose solution (99% ^{13}C isotopic enrichment, Sigma–Aldrich, Buchs, Switzerland) was prepared for injections in awake mice. Unless otherwise specified, the injections were intraperitoneal (i.p.). A series of doses corresponding to 1 mg/g were delivered at several time points and mice were euthanized at different times according to the following schemes: at t = 10 min after a single injection at t = 0; at t = 30 min (injections at t = 0 and 10 min); at t = 60 min (injections at t = 0, 10, and 20 min; at t = 120 min (injections at t = 0, 10, 20, 60 and 90 min); and at t = 180 min (injections at 0, 10, 20, 60, 90, 120, and 150 min). A different scheme was used for experiments performed over 48 h, in which mice were fasted overnight with free access to water and, for the following 48 h, the only source of exogenous carbon provided to the animals was a 0.55 M aqueous [U-^{13}C]glucose solution administered orally *ad libitum*.

2.2. EM sample preparation and imaging

Tissue preparation for EM was performed according to established procedures (Knott et al., 2002). Each mouse was deeply anesthetized by an i.p. injection of sodium pentobarbital (60 mg/kg). Isotonic phosphate buffered saline (10 ml) was perfused *via* the heart followed immediately by 200 ml of 2.5% glutaraldehyde and 2% paraformaldehyde in phosphate buffer (0.1 M, pH 7.4). Two hours after perfusion, the brain was removed, and 70 μm-thick vibratome sections cut (Leica VT1200; Leica Microsystems). These sections were washed in cacodylate buffer (0.1 M, at pH 7.4), post-fixed for 40 min in 1.5% potassium ferrocyanide and 1% osmium tetroxide, followed by 1 h in 1% osmium tetroxide alone using the same buffer, then in 1% uranyl acetate in water for 40 min. The sections were then dehydrated in ethanol and finally infiltrated with Durcupan ACM resin (Fluka, Buchs, Switzerland). The sections were flat-embedded between glass slides and left for 24 h at 65 °C for the resin to harden. Series of 70 nm thin sections were cut with an ultra-microtome, placed on EM slot grids with a Pioloform support and carbon coated film and imaged in a transmission electron microscopy (Tecnai Spirit, FEI Company) operated at 80 kV. For large size maps of the motor cortex, grids were imaged with a scanning electron microscope (Helios 650, FEI Company) using the STEM III detector. For imaging, the following settings were used: 30 keV acceleration voltage, 800 pA beam current, immersion lens setting, 1 μs dwell time, 6144 × 4096 pixel frame size, 5–15 nm pixel size, 5–6 mm working distance. The images were recorded either in the bright field or high-angle annular dark field mode. Imaging was driven by the Maps software (FEI Company) (Fonta et al., 2015), and stitched images as large as 1.66 × 0.2 mm^2 were acquired.

2.3. NanoSIMS imaging and analysis

After EM imaging, thin sections were mounted on 10 mm diameter, aluminum mounts with double-sided copper sticking tape, and coated with a 10 nm layer of gold. The distribution of C isotopes (*i.e.* the $^{13}C/^{12}C$ ratio) was determined in the same areas with a NanoSIMS 50L instrument, following established procedures (Takado et al., 2015; Kopp et al., 2013, 2015; Pernice et al., 2012). Briefly, a Cs^+ beam (1–5 pA) was focused to a spot size of about 100–300 nm, depending on the spatial resolution needed, and rastered across areas typically 40 by 40 μm^2 (256 by 256 pixels) for mosaic images and 10–30 by 10–30 μm^2 (128 by 128 or 256 by 256 pixels) for high resolution imaging. This created secondary ions that were separated by the mass spectrometer and counted individually and simultaneously (multi-collection) in electron multipliers at a mass resolution sufficient to resolve all potential mass-interferences. Maps of the carbon isotopic ratio distribution can be obtained as ratios between the following ion images: $^{13}C^{14}N^-/^{12}C^{14}N^-$. Enrichments in ^{13}C are reported in the delta-notation, as deviation in parts-per-thousand from brain tissue with normal carbon isotopic composition:

$$\delta^{13}C\,(‰) = \left(\frac{C_{mes}}{C_{nat}} - 1\right) \times 1000,$$

where C_{mes} is the measured $^{13}C/^{12}C$ ratio of a given pixel in the NanoSIMS map and C_{nat} is the average natural $^{13}C/^{12}C$ ratio in non-labeled, identically prepared brain tissue measured regularly throughout the period of NanoSIMS analyses (0.01112 ± 0.0001 (1 SD), n = 49). The ions $^{31}P^-$ and $^{32}S^-$ were also collected in some imaging sessions. NanoSIMS images were processed with the L'IMAGE© software; count-rate smoothing (3 by 3 pixels) was systematically applied to all images. By overlaying a semi-transparent NanoSIMS image over an electron micrograph of the same region, it is possible to assign individual pixels in the NanoSIMS image to specific cell types or their sub-cellular compartments. Quantified $\delta^{13}C$ enrichments can therefore be ascribed to each structure.

A thin section (area 1.2 × 0.15 mm^2) of the primary motor cortex, cut in the coronal plane containing all six cortical layers was imaged in the EM. The same region was imaged in the NanoSIMS and the $\delta^{13}C$ spatial distribution mapped. From the EM images, neurons and astrocytes were identified according to their morphology. Microglial were not included, and could be easily identified based on their densely stained nuclei and cytoplasm, and their size. Quantified ^{13}C enrichments were therefore separately assigned to each single neuron and astrocyte. A statistical analysis was performed on all identified astrocytes and neurons imaged by NanoSIMS (17 glial cells) in each of the 6 cortical layers. Following the identification of each cell nucleus and membrane on high-resolution images, two compartments were defined for each cell: the cell nucleus and the cytoplasm, the latter being defined as the region between the nuclear envelope and the cell membrane, therefore including Golgi apparatus, endothelial reticulum, and mitochondria. For all tissue sections imaged by EM and NanoSIMS, an additional statistical analysis was performed to determine the average $\delta^{13}C$ in each cell nucleus and cytoplasm separately.

Statistical analyses were performed with the software OriginPro 9.0G. Kolmogorov–Smirnov test was first conducted to check the data for normality. Significance between two variables was analyzed by the Student's t-test. For the statistical analysis of multiple groups, one-way ANOVA was used followed by Tukey's test. Results were considered significant at the 5% level. Unless otherwise stated, values given are means ±1 SD. Error bars show ±1 SD throughout the paper.

3. Results

As can be clearly seen in the EM and corresponding NanoSIMS mosaic images of the coronal section through motor cortex (Fig. 1A) and in the magnified part of layer V (Fig. 1B), both neurons and astrocytes were clearly enriched in ^{13}C. The analysis of the average ^{13}C enrichment over both cell types shows significantly higher $\delta^{13}C$ in the neurons of all layers compared to the astrocyte population in this region of the cortex ($p < 0.05$). Variations in the levels were apparent between the neurons of the different layers with layer V showing the highest $\delta^{13}C$ (Fig. 1C).

Further analysis at higher resolution explored the spatial distribution of the ^{13}C enrichment within each individual cell (Fig. 2A and B). The average $\delta^{13}C$ in the nucleus and the cytoplasm of both astrocytes and neurons was obtained as a function of time (Fig. 2C). Both compartments showed less ^{13}C-enrichment in astrocytes than in neurons. In neurons, the enrichment in the cytoplasm and the nucleus was found to increase at a similar rate whereas in astrocytes the enrichment increased at a significantly lower rate in the nucleus than in the cytoplasm. The $\delta^{13}C$ value after 180 min was twice as large in the neuronal nuclei as compared to the astrocyte nuclei.

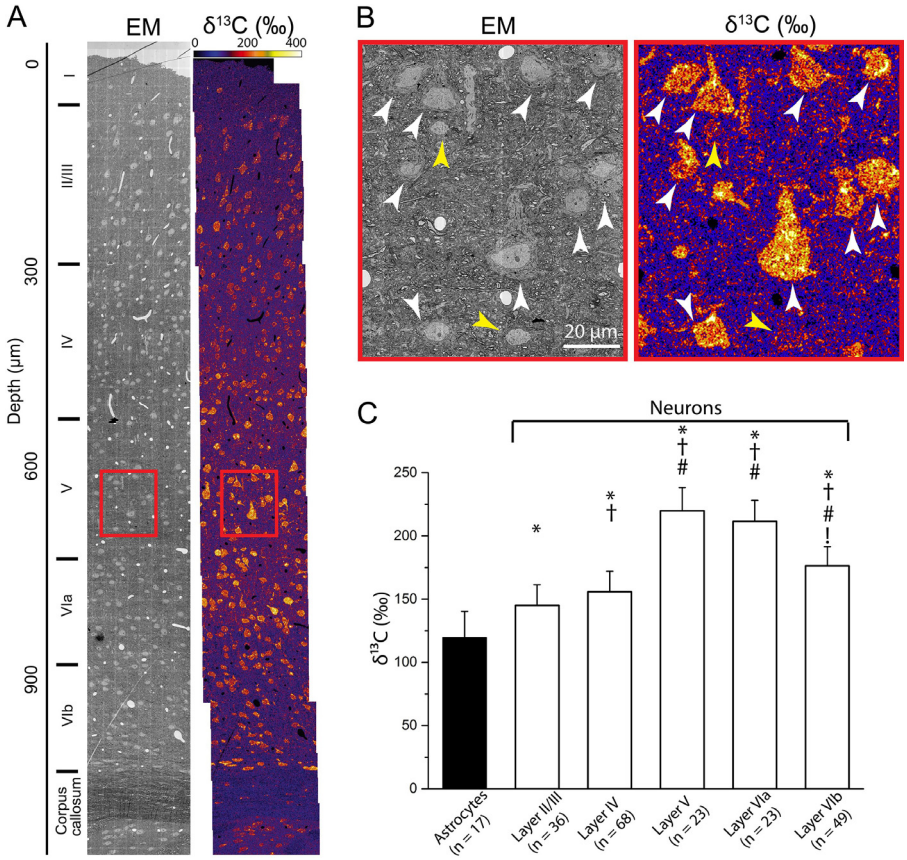

Fig. 1. ^{13}C-enrichment map in a coronal section through motor cortex of a healthy adult mouse after a 3 h labeling period with [U-^{13}C]glucose i.p. injections (see Section 2); (A) large-scale EM image (1.2 × 0.15 mm^2) and corresponding δ^{13}C NanoSIMS mosaic image. The cortical layers are indicated with roman numbers; (B) Magnified EM and NanoSIMS δ^{13}C-maps from layer V, as indicated in A. White arrowheads point to neurons and yellow arrowheads point to astrocytes; (C) Quantified ^{13}C-enrichments in astrocytes, averaged over the entire cortical thickness, and in neurons, averaged over each layer; the following statistical parameters were obtained using one-way ANOVA followed by Tukey's test: $F = 127.5$, $^{*}p < 0.05$ *vs* astrocyte, $^{\dagger}p < 0.05$ *vs* layer II/III, $^{\#}p < 0.05$ *vs* layer IV, $^{!}p < 0.05$ *vs* layer V. (For interpretation of the references to colour in this figure legend, the reader is referred to the web version of this article.)

To investigate in more depth the labeling pattern in cell nuclei, the ^{31}P (100% natural abundance) and ^{32}S (95% natural abundance) spatial distribution were recorded in addition to the δ^{13}C map and EM image in individual neocortical neurons identified in brain sections prepared from mice labeled from oral administration of [U-^{13}C]glucose over 48 h (Fig. 3A). Even without using the clear structural definition provided by EM imaging, the nucleolus can be unequivocally distinguished from adjacent chromatin packages based on the strong image contrast provided by the ^{32}S/^{12}C and ^{31}P/^{12}C maps. The ^{31}P/^{12}C, ^{32}S/^{12}C, and δ^{13}C ratios are shown along specific line profiles crossing chromatin packages, nucleoplasm, and the nucleolus, respectively (Fig. 3B). The nucleoplasm is characterized by a low ^{31}P/^{12}C ratio. Furthermore, the ^{31}P/^{12}C ratio measured in the nucleolus is smaller than in the chromatin packages. Statistical analysis of a series of adjacent nucleolus and chromatin packages in neurons leads to a quantitative difference of a factor of 2.0 ± 0.2 ($n = 10$), which is consistent with the compositional difference between double-stranded DNA, mostly located in chromatin, and single-stranded RNA that forms a large part of the nucleolus (Fig. 3B). In addition, because nucleic acids do not contain S atoms, the substantially higher ^{32}S/^{12}C ratios observed in the nucleoli is a signature of its larger protein content compared with the chromatin packages. The fact that a relatively large ^{32}S/^{12}C is a proxy for a high concentration of proteins was previously established (Quintana et al., 1987). As was already apparent in the images obtained after shorter labeling periods (see Fig. 2A), the neuronal nucleolus exhibits a ^{13}C enrichment that is considerably larger than in the other cell compartments and more than in any in other nuclear structure.

4. Discussion

4.1. Fundamental considerations for the interpretation of NanoSIMS δ^{13}C images

There are a number of considerations that must be taken into account when interpreting high-resolution NanoSIMS images in the context of metabolic studies using ^{13}C-labeled substrates. First, although the NanoSIMS isotopic images provide precise isotopic quantification (relative to a sample of known isotopic composition) and relative atomic compositions with high spatial resolution (see *e.g.* Fig. 3), they do not contain information about the molecular chemistry of the specific molecules (isotopically enriched or not) present in the samples. Molecular identity has to be obtained with other techniques, or indirectly deduced from the structural information provided by EM imaging. A second consideration is related to sample preparation. Fixation of the brain tissue with glutaraldehyde and paraformaldehyde solutions, staining procedures, dehydration with alcohol, and epoxy resin embedding will likely wash out the water-soluble compounds. These include [U-^{13}C]glucose and its direct soluble catabolic products such as lactate, glutamate, and glutamine. Trace amounts of soluble compounds left in the sample after normal sample preparation are most likely below the detection limit of the NanoSIMS (δ^{13}C > 50‰). This was demonstrated by the absence of detectable ^{13}C-enrichment in neocortex obtained from animals that were euthanized shortly (10 min or less) after the intravenous (i.v.) injection of 1 mg/g of [U-^{13}C]glucose (data not shown).

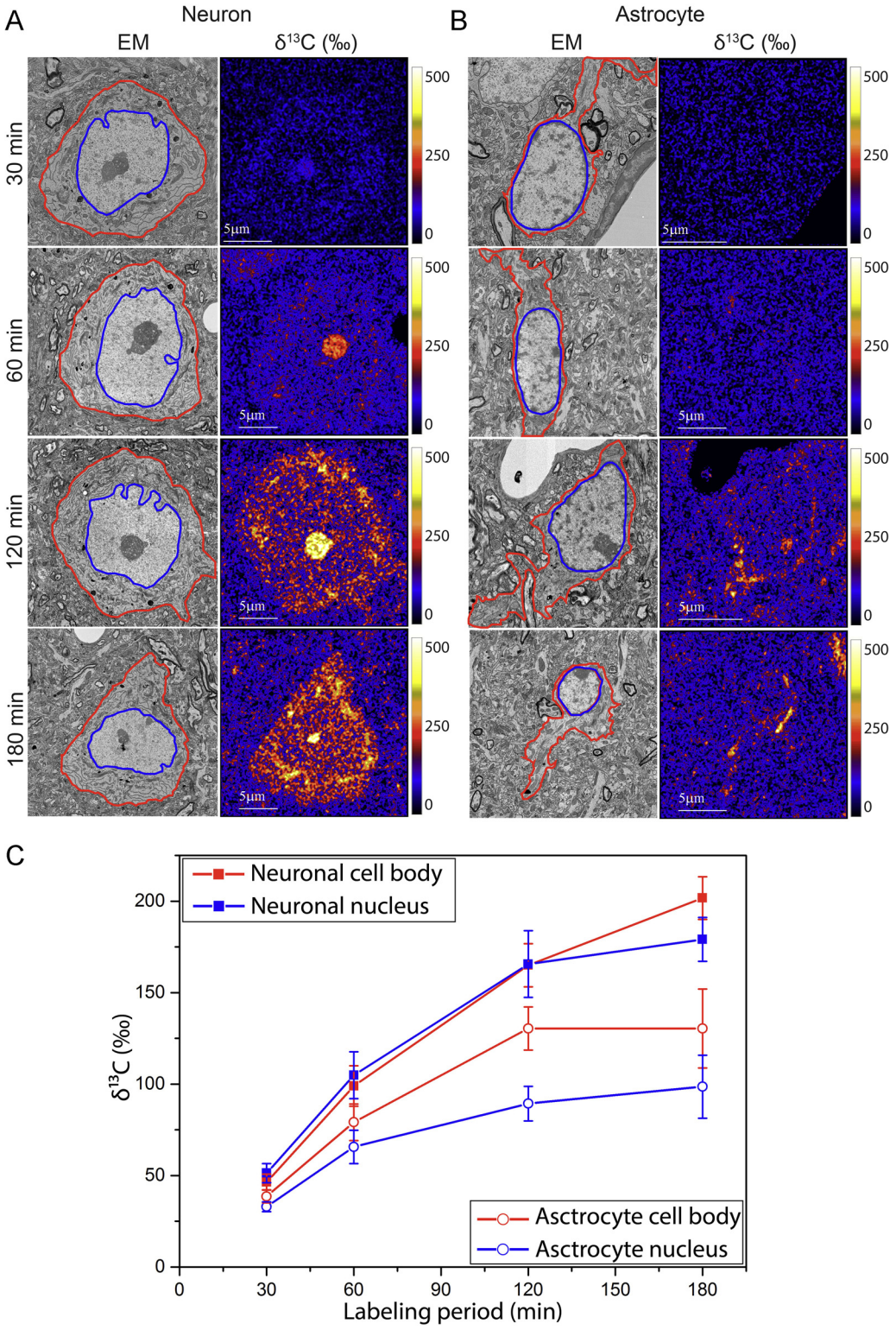

Fig. 2. Evolution of the ^{13}C enrichment in layer V neurons (n = 23) and astrocytes (located across the cortex, n = 17). The nuclear envelope of the cells is highlighted with a thick blue curve and the cell membrane with a thick red curve; (A) EM images and corresponding $\delta^{13}C$ NanoSIMS maps of individual neurons; (B) EM images and corresponding $\delta^{13}C$ NanoSIMS maps of individual astrocytes; (C) ^{13}C enrichment as a function of time in the cytoplasm and the nucleus of both cell types. Between 10 and 15 cells were analyzed for each time point. (For interpretation of the references to colour in this figure legend, the reader is referred to the web version of this article.)

Therefore, despite the fact that the molecular origin of the detected ^{13}C-enrichments is unknown, it is likely that the isotopic enrichments primarily arises from macromolecular structures, such as proteins, lipids, and nucleic acids, which are trapped during the polymerization caused by the chemical fixatives, and immobilized and preserved during sample preparation. A third consideration related to the use of stable isotopes, is that ^{13}C-labeling of small metabolites does not interfere with their biological function. This is in contrast with other approaches, such as *e.g.* fluorescent tags. The process of injecting [U-^{13}C]glucose

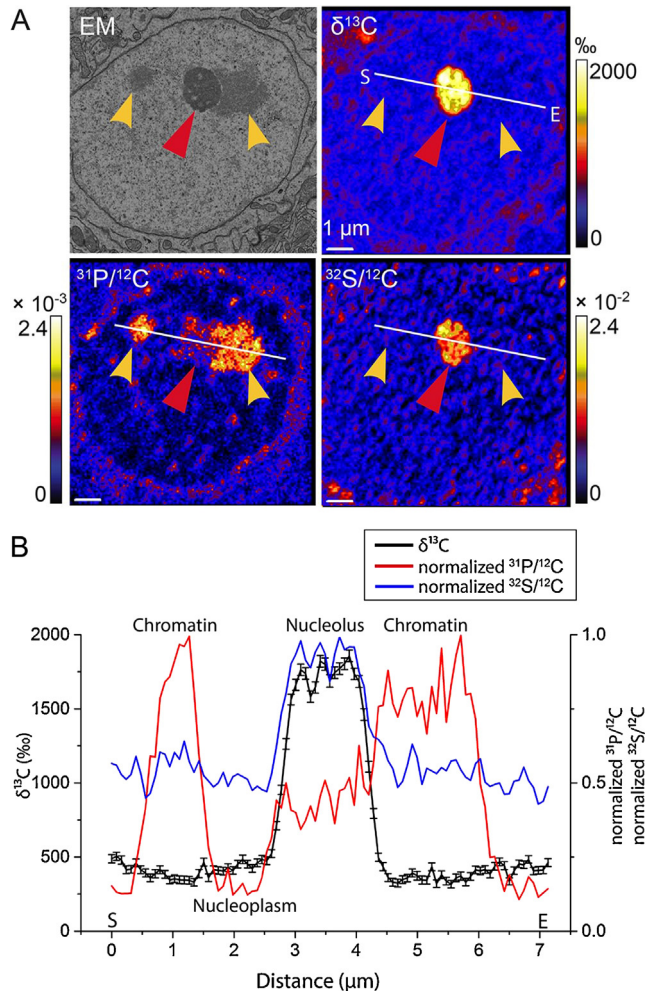

Fig. 3. ^{13}C enrichment in a neuronal nucleus located in mouse cortical layer V labeled from oral administration of [U-^{13}C]glucose over 48 h; (A) EM image (upper left) and corresponding NanoSIMS images: $\delta^{13}C$ (upper right), $^{31}P/^{12}C$ (lower left), $^{32}S/^{12}C$ (lower right), respectively. Red arrowheads point to nucleolus and yellow arrowheads point to chromatin; (B) line profiles across nucleoplasm, nucleolus, and chromatin structures, along the trajectory indicated in (A). (For interpretation of the references to colour in this figure legend, the reader is referred to the web version of this article.)

does induce some level of stress on the mouse, but the cellular-level biochemistry associated with glucose metabolism otherwise proceeds naturally, including biosynthesis of macromolecular structures.

Within this established framework and the reasonable assumption that the isotopic ratio in the ultrastructure of different cell types or subcellular compartments is not altered by sample preparation procedures, the capability of the NanoSIMS to quantitatively measure the $^{13}C/^{12}C$ ratio with high spatial resolution allows for a direct comparison of local cellular metabolic activity in specific regions of the brain.

4.2. Spatial distribution of the cerebral ultrastructure ^{13}C-enrichment

The significantly larger ^{13}C enrichment measured in layer V of motor cortex compared to layer IV (Fig. 1) shows similarity with the local cerebral glucose utilization ($LCMR_{Glu}$) measured in rat motor cortex by autoradiography following the injection of [^{14}C]2-deoxy-D-glucose (Wree et al., 1990). However, this does not mean that the measured ^{13}C spatial distribution reported here is a measure of the $LCMR_{Glu}$. The NanoSIMS measurements provide a map of the local cellular metabolic activity while 2-deoxy-D-glucose is not significantly metabolized on the time scale of the experiments, and the autoradiography experiments with [^{14}C]glucose have shown that the results may strikingly differ from those obtained with [^{14}C]2-deoxy-D-glucose (Ackermann and Lear, 1989; Adachi et al., 1995).

4.3. Nucleus ^{13}C-enrichment as a probe of local cellular metabolic activity

The turnover of nucleotides and nucleotide proteins is most likely at the origin of the very large ^{13}C enrichment observed in the brain cell nuclei. The biosynthesis of RNA and nucleotide proteins from ^{13}C-glucose has previously been studied *in vitro* in cancer cells, where it was shown that essentially all nucleotide riboses originate from glucose,(Boros et al., 1997; Fan et al., 2012) but so far this has not yet been investigated in detail in brain cells. The ^{13}C-enrichment maps provided by the NanoSIMS can therefore be considered as a measure of the local cellular cerebral metabolic activity that takes place *via* biosynthetic pathways. Since neurons are not gluconeogenic (Hertz et al., 2007), the ^{13}C that is incorporated into their nucleus must originate from ^{13}C-glucose or its soluble metabolites. In other words, a substantial fraction of ^{13}C glucose entering the brain is used for the biosynthesis of nucleotides and nucleotide proteins in neurons. In astrocytes, the rate of ^{13}C incorporation into the nucleus is considerably lower than into the cytoplasm, whereas in neurons these two rates are similar (Fig. 2). This indicates that the fate of glucose in the glial compartment is different than in neurons, as expected from previous studies (Hertz et al., 2007).

4.4. Neuronal vs glial ^{13}C enrichment

Various pieces of evidence suggest an important interplay between neurons and astrocytes in the uptake and utilization of glucose (Belanger et al., 2011; Nehlig and Coles, 2007). However, no techniques have so far been able to measure and compare the extent to which glucose is metabolized by these cells *in vivo* and in which parts of the cell. Our observation that ^{13}C enrichment in neuronal nuclei is about twice as high as in astrocytic nuclei indicates a lower local cellular metabolic activity in the glial compartment.

A straightforward interpretation of our results would be that neurons take up more glucose than astrocytes, as supported by several studies, including a model based on measured concentrations and kinetic parameters of glucose and monocarboxylate transporters (Simpson et al., 2007). Recently, *in vitro* experiments on immature cultured cells and slices showed that astrocytes take up and metabolize glucose analogs at a considerably higher rate (Jakoby et al., 2014). If this holds for the adult tissue, *in vivo*, it poses the question as to why we see greater ^{13}C incorporation in neurons at all time points. Several lines of evidence have suggested a net transfer of metabolites from astrocytes to neurons (Hertz, 1979; Pellerin and Magistretti, 1994), and the current observations could be a reflection of this. The rate at which ^{13}C is released as $^{13}CO_2$ is several times slower in astrocytes than in neurons,(Abe et al., 2006) therefore a significant amount of ^{13}C could exit astrocytes in the form of other soluble metabolites. It is well established that a main fate of glucose in astrocytes is the synthesis of glutamine as well as lactate (Schousboe et al., 2013). Because we observe that a large amount of ^{13}C derived from the injected [U-^{13}C]glucose is used to form nucleotides, the overall higher level of incorporation of ^{13}C into neuronal cytoplasm compared to astrocytic (about 50% higher after 3 h) indicates that, unless the majority of ^{13}C-labeled metabolites are released from astrocytes into the blood pool and

exit the brain, at least part of this ^{13}C would be transferred from astrocytes to neurons.

However, we acknowledge that our observations do not provide direct evidence for transfer of soluble, ^{13}C-labeled metabolites from astrocytes to neurons. The required sample preparation technique is preferentially capturing larger, insoluble molecules, preventing direct conclusions about relative concentrations of the more soluble and labile components, such as lactate and glutamine.

Overall, the present study demonstrates that *in vivo* local cerebral metabolic activity can be quantitatively probed with an unprecedented spatial resolution through the rate of incorporation of carbon atoms from the backbone of [U-^{13}C]glucose into cellular ultrastructure *via* biosynthetic pathways.

Authors' contribution

Y.T., G.K., B.M.H., A.M. and A.C. designed the study. Y.T. and G.K. performed the animal labeling experiments and prepared the samples for imaging. Y.T., G.K., and B.H.M. did the EM imaging experiments. Y.T., S.E., and A.M. performed the NanoSIMS experiments. Y.T., G.K., B.M.H., M.M., and A.M. analyzed the data. Y.T. performed the statistical analyses. A.C. wrote the manuscript. All authors discussed the results and commented on the manuscript.

Conflict of interest

The authors declare no conflict of interest.

Acknowledgements

The authors would like to thank Dr. Céline Loussert (Electron Microscope Facility at University of Lausanne) for expert advice and technical assistance, as well as Ben Lich and Cliff Mathisen (FEI Company, Eindhoven, The Netherlands) for fruitful discussions. We also thank Dr. Stanislav Fakan for helpful insights on nuclear ultrastructure and biology.

References

Abe, T., Takahashi, S., Suzuki, N., 2006. Oxidative metabolism in cultured rat astroglia: effects of reducing the glucose concentration in the culture medium and of D-aspartate or potassium stimulation. J. Cereb. Blood Flow Metab. 26, 153–160.

Ackermann, R.F., Lear, J.L., 1989. Glycolysis-induced discordance between glucose metabolic rates measured with radiolabeled fluorodeoxyglucose and glucose. J. Cereb. Blood Flow Metab. 9, 774–785.

Adachi, K., Cruz, N.F., Sokoloff, L., Dienel, G.A., 1995. Labeling of metabolic pools by [6-C-14]Glucose during K^+-induced stimulation of glucose-utilization in rat-brain. J. Cereb. Blood Flow Metab. 15, 97–110.

Austin, L., Brown, J.G., Carter, J.G., Lowry, O.H., 1972. Turnover of protein in discrete areas of rat-brain. Biochem. J. 126, 351–359.

Belanger, M., Allaman, I., Magistretti, P.J., 2011. Brain energy metabolism: focus on astrocyte-neuron metabolic cooperation. Cell Metab. 14, 724–738.

Ben-Yoseph, O., Camp, D.M., Robinson, T.E., Ross, B.D., 1995. Dynamic measurements of cerebral pentose-phosphate pathway activity in-vivo using [1,6-c-13(2),6,6-h-2(2)]glucose and microdialysis. J. Neurochem. 64, 1336–1342.

Boros, L.G., Puigjaner, J., Cascante, M., Lee, W.N.P., Brandes, J.L., Bassilian, S., et al., 1997. Oxythiamine and dehydroepiandrosterone inhibit the nonoxidative synthesis of ribose and tumor cell proliferation. Cancer Res. 57, 4242–4248.

Brekke, E.M., Walls, A.B., Schousboe, A., Waagepetersen, H.S., Sonnewald, U., 2012. Quantitative importance of the pentose phosphate pathway determined by incorporation of ^{13}C from [2-13C]- and [3-13C]glucose into TCA cycle intermediates and neurotransmitter amino acids in functionally intact neurons. J. Cereb. Blood Flow Metab. 32, 1788–1799.

Devor, A., Sakadzic, S., Srinivasan, V.J., AYaseen, M., Nizar, K., Saisan, P.A., et al., 2012. Frontiers in optical imaging of cerebral blood flow and metabolism. J. Cereb. Blood Flow Metab. 32, 1259–1276.

Dienel, G.A., Wang, R.Y., Cruz, N.F., 2002. Generalized sensory stimulation of conscious rats increases labeling of oxidative pathways of glucose metabolism when the brain glucose-oxygen uptake ratio rises. J. Cereb. Blood Flow Metab. 22, 1490–1502.

Fan, T.W.M., Tan, J.L., McKinney, M.M., Lane, A.N., 2012. Stable isotope resolved metabolomics analysis of ribonucleotide and RNA metabolism in human lung cancer cells. Metabolomics 8, 517–527.

Fonta, C.L., Leis, A., Mathisen, C., Bouvier, D.S., Blanchard, W., Volterra, A., et al., 2015. Analysis of acute brain slices by electron microscopy: a correlative light-electron microscopy workflow based on Tokuyasu cryo-sectioning. J. Struct. Biol. 189, 53–61.

Hertz, L., 1979. Functional interactions between neurons and astrocytes.1. Turnover and metabolism of putative amino-acid transmitters. Prog. Neurobiol. 13, 277–323.

Hertz, L., Peng, L., Dienel, G.A., 2007. Energy metabolism in astrocytes: high rate of oxidative metabolism and spatiotemporal dependence on glycolysis/glycogenolysis. J. Cereb. Blood Flow Metab. 27, 219–249.

Hoppe, P., Cohen, S., Meibom, A., 2013. NanoSIMS: technical aspects and applications in cosmochemistry and biological geochemistry. Geostand. Geoanal. Res. 37, 111–154.

Jakoby, P., Schmidt, E., Ruminot, I., Gutierrez, R., Barros, L.F., Deitmer, J.W., 2014. Higher transport and metabolism of glucose in astrocytes compared with neurons: a multiphoton study of hippocampal and cerebellar tissue slices. Cereb. Cortex 24, 222–231.

Jin, T., Mehrens, H., Hendrich, K.S., Kim, S.-G., 2014. Mapping brain glucose uptake with chemical exchange-sensitive spin-lock magnetic resonance imaging. J. Cereb. Blood Flow Metab. 34, 1402–1410.

Knott, G.W., Quairiaux, C., Genoud, C., Welker, E., 2002. Formation of dendritic spines with GABAergic synapses by whisker stimulation in induced adult mice. Neuron 34, 265–273.

Kopp, C., Pernice, M., Domart-Coulon, I., Djediat, C., Spangenberg, J.E., Alexander, D.T.L., et al., 2013. Highly dynamic cellular-level response of symbiotic coral to a sudden increase in environmental nitrogen. mBio 4,, e00052-13.

Kopp, C., Domart-Coulon, I., Escrig, S., Humbel, B.M., Hignette, M., Meibom, A., 2015. Subcellular investigation of photosynthesis-driven carbon assimilation in the symbiotic reef coral pocillopora damicornis. mBio 6, e02299–e2314.

Lechene, C., Hillion, F., McMahon, G., Benson, D., Kleinfeld, A.M., Kampf, J.P., et al., 2006. High-resolution quantitative imaging of mammalian and bacterial cells using stable isotope mass spectrometry. J. Biol. 5, 20.

Nehlig, A., Coles, J.A., 2007. Cellular pathways of energy metabolism in the brain: is glucose used by neurons or astrocytes? Glia 55, 1238–1250.

Pellerin, L., Magistretti, P.J., 1994. Glutamate uptake into astrocytes stimulates aerobic glycolysis – a mechanism coupling neuronal-activity to glucose-utilization. Proc. Natl. Acad. Sci. U. S. A. 91, 10625–10629.

Pernice, M., Meibom, A., Van Den Heuvel, A., Kopp, C., Domart-Coulon, I., Hoegh-Guldberg, O., et al., 2012. A single-cell view of ammonium assimilation in coral-dinoflagellate symbiosis. ISME J. 6, 1314–1324.

Quintana, C., Olmedilla, A., Antoine, N., Ollacarizqueta, A., 1987. The occurrence of metals Al, Fe, Ni, Cu, Zn in the nuclei of animal-cells – an ultrastructural, insitu X-ray Microanalytical Study. Biol. Cell 61, 115–119.

Schmidt, K.C., Smith, C.B., 2005. Resolution, sensitivity and precision with autoradiography and small animal positron emission tomography: implications for functional brain imaging in animal research. Nucl. Med. Biol. 32, 719–725.

Schousboe, A., 2012. Studies of brain metabolism: a historical perspective. In: Choi, I.-Y., Gruetter, R. (Eds.), Neural Metabolism In Vivo, vol. 4. Springer, New York, NY, pp. 909–920.

Schousboe, A., Bak, L.K., Waagepetersen, H.S., 2013. Astrocytic control of biosynthesis and turnover of the neurotransmitters glutamate and GABA. Front. Endocrinol. (Lausanne) 4, 102.

Simpson, I.A., Carruthers, A., Vannucci, S.J., 2007. Supply and demand in cerebral energy metabolism: the role of nutrient transporters. J. Cereb. Blood Flow Metab. 27, 1766–1791.

Sokoloff, L., Reivich, M., Kennedy, C., Desrosiers, M.H., Patlak, C.S., Pettigrew, K.D., et al., 1977. Deoxyglucose-C-14 method for measurement of local cerebral glucose-utilization – theory procedure, and normal values in conscious and anesthetized albino-rat. J. Neurochem. 28, 897–916.

Takado, Y., Knott, G., Humbel, B.M., Escrig, S., Masoodi, M., Meibom, A., et, al., 2015. Imaging liver and brain glycogen metabolism at the nanometer scale. Nanomed. Nanotechnol. 11, 239–245.

Vrba, R., 1962. Glucose metabolism in rat brain in vivo. Nature 195, 663–665.

Vrba, R., 1964. Utilization of glucose carbon in vivo in mouse. Nature 202, 247–249.

Walker-Samuel, S., Ramasawmy, R., Torrealdea, F., Rega, M., Rajkumar, V., Johnson, S.P., et al., 2013. In vivo imaging of glucose uptake and metabolism in tumors. Nat. Med. 19, 1067–1072.

Wehrl, H.F., Hossain, M., Lankes, K., Liu, C.C., Bezrukov, I., Martirosian, P., et al., 2013. Simultaneous PET-MRI reveals brain function in activated and resting state on metabolic, hemodynamic and multiple temporal scales. Nat. Med. 19, 1184–1189.

Wree, A., Zilles, K., Schleicher, A., 1990. Local cerebral glucose-utilization in the neocortical areas of the rat-brain. Anat. Embryol. 181, 603–614.